

**Comparison
of ultrasound signs, computed
tomography data and morphological
examination of the lungs in patients
with coronavirus infection:
post hoc analysis**

R.E. Lakhin^{1,*}, E.A. Zhirnova², A.V. Shchegolev¹,
I.S. Zheleznyak¹, V.S. Chirsky¹, D.Y. Pluminsky¹

¹ Military Medical Academy, St. Petersburg, Russia

² Saint-Petersburg State University Hospital, St. Petersburg,
Russia

**Сопоставление
ультразвуковых признаков,
данных компьютерной томографии
и морфологического исследования
легких у пациентов с коронавирусной
инфекцией: *post hoc* анализ**

Р.Е. Лахин^{1,*}, Е.А. Жирнова², А.В. Щеголев¹,
И.С. Железняк¹, В.С. Чирский¹, Д.Ю. Пламинский¹

¹ ФГБВОУ ВО «Военно-медицинская академия

им. С.М. Кирова» МО РФ, Санкт-Петербург, Россия

² Клиника высоких медицинских технологий

им. Н.И. Пирогова Санкт-Петербургского
государственного университета, Санкт-Петербург,
Россия

Abstract

INTRODUCTION: Ultrasound examination (US) of the lungs has shown high efficiency in the diagnosis of COVID-19 pneumonia. The aim of the research was studying the correspondence of computed tomography (CT) US signs of the lungs and morphological data in patients with COVID-19 pneumonia. **MATERIALS AND METHODS:** The *post hoc* analysis included 388 patients who simultaneously underwent ultrasound and CT of the lungs. Lung ultrasound was performed according to the 16-zone "Russian Protocol". Morphological data were obtained from the results of pathoanatomic examination of deceased patients. **RESULTS:** The comparison of signs detected by CT and ultrasound of the lungs was performed during a multidimensional correspondence analysis. The analysis was carried out using a three-dimensional solution that explained 64.9% of inertia ($p < 0.001$). CT signs of "ground glass opacity" (100%) corresponded to the B-line at ultrasound (100%), CT of the consolidation sign (44.8%) — ultrasound signs of consolidation (46.9%), aerobronchogram of CT (34%) — aerobronchogram of ultrasound (36.9%), free liquid CT (11.1%) — free liquid Ultrasound (13.9%). CT signs of reticular changes (29.6%) and "cobblestone pavement" (12.4%) corresponded to various combinations of ultrasound signs of subpleural consolidation and B-lines. The B-lines were caused by the exudation of fluid

Реферат

АКТУАЛЬНОСТЬ: Ультразвуковое исследование (УЗИ) легких показало высокую эффективность в диагностике пневмонии при коронавирусной инфекции (COVID-19). **ЦЕЛЬ ИССЛЕДОВАНИЯ:** Изучение соответствий признаков, определяемых при УЗИ легких, с признаками компьютерной томографии (КТ) и морфологическими данными у пациентов с пневмонией COVID-19. **МАТЕРИАЛЫ И МЕТОДЫ:** В *post hoc* анализ было включено 388 пациентов, которым одновременно было выполнено УЗИ и КТ легких. УЗИ легких проводили согласно 16-зонному «Русскому протоколу». Морфологические данные получены по результатам патологоанатомического исследования умерших пациентов. Гистологические срезы окрашивали гематоксилином и эозином, а затем исследовали под световым микроскопом. **РЕЗУЛЬТАТЫ:** Сопоставление признаков, выявляемых с помощью КТ и УЗИ легких, выполнено в ходе многомерного анализа соответствий. Анализ был проведен с помощью трехмерного решения, которое объясняло 64,9% инерции ($p < 0,001$). КТ-признаку «матового стекла» (100%) соответствовали В-линии при УЗИ (100%), КТ-признаку консолидации (44,8%) — ультразвуковые (УЗ) признаки консолидации (46,9%), аэробронхограмме КТ (34%) — аэробронхограмма УЗИ



and protein molecules into the intraalveolar space against the background of massive death of alveolocytes and formed by the development of intraalveolar edema and the formation of hyaline membranes. The ultrasonic sign of consolidation appeared in the airless zone of the lungs. Subpleural consolidation are caused by thickening and inflammatory infiltration of the pleura, diffuse alveolar damage, with intraalveolar edema, death and decay of alveolocytes, perivascular inflammatory cell reaction/ During treatment for more than 7 days, consolidation in the lung tissue developed due to the disorganization of the organ structure due to the progression of fibrosis. **CONCLUSIONS:** Multivariate correspondence analysis showed correlation of CT signs and US signs of the lungs. Morphological analysis showed polymorphism of histological data that caused the formation of ultrasound signs.

KEYWORDS: coronavirus infection, COVID-19, ultrasonography, tomography; pneumonia, pathology

* *For correspondence:* Roman E. Lakhin — Dr. Med. Sci., professor, Department of Anesthesiology and Intensive Care, Military Medical Academy, St. Petersburg, Russia; e-mail: doctorlahin@yandex.ru

☑ *For citation:* Lakhin R.E., Zhirnova E.A., Shchegolev A.V., Zheleznyak I.S., Chirsky V.S., Pluminsky D.Y. Comparison of ultrasound signs, computed tomography data and morphological examination of the lungs in patients with coronavirus infection: *post hoc* analysis. *Annals of Critical Care*. 2023;3:82–96. <https://doi.org/10.21320/1818-474X-2023-3-82-96>

📅 *Received:* 01.02.2023

📅 *Accepted:* 03.06.2023

📅 *Published online:* 28.07.2023

(36,9%), свободной жидкости КТ (11,1%) — свободная жидкость УЗИ (13,9%). КТ-признакам ретикулярных изменений (29,6%) и «бульжной мостовой» (12,4%) соответствовали различные комбинации УЗ-признаков субплевральной консолидации и В-линий. В экссудативной фазе В-линии были обусловлены пропотеванием жидкости и белковых молекул во внутриальвеолярное пространство на фоне массивной гибели альвеолоцитов и поражением эндотелия капилляров. В ранней пролиферативной фазе В-линии были сформированы развитием внутриальвеолярного отека и образованием гиалиновых мембран. УЗ-признак консолидации появлялся в безвоздушной зоне легких. Небольшие зоны субплевральной консолидации обусловлены утолщением и воспалительной инфильтрацией плевры, диффузным альвеолярным повреждением, с гибелью и спаданием альвеолоцитов, периваскулярной воспалительно-клеточной реакцией. Большие объемы консолидации в экссудативной фазе формировались за счет внутриальвеолярного отека, наложений десквамированного альвеолярного эпителия и макрофагами в просветах альвеол. При лечении более 7 суток в легочной ткани формировались признаки дезорганизации структуры органа за счет развивающегося фиброза. **ВЫВОДЫ:** Многомерный анализ соответствий показал связь признаков, выявляемых с помощью КТ и УЗИ легких. Морфологический анализ показал полиморфность гистологических данных, обусловивших формирование ультразвуковых признаков.

КЛЮЧЕВЫЕ СЛОВА: коронавирусная инфекция, COVID-19, ультразвуковое исследование, компьютерная томография; пневмония, патологическая анатомия

* *Для корреспонденции:* Лажин Роман Евгеньевич — д-р мед. наук, профессор кафедры военной анестезиологии и реаниматологии ФГБВОУ ВО «Военно-медицинская академия им. С.М. Кирова» МО РФ, Санкт-Петербург, Россия; e-mail: doctor-lahin@yandex.ru

☑ *Для цитирования:* Лажин Р.Е., Жирнова Е.А., Щеголев А.В., Железняк И.С., Чирский В.С., Пламинский Д.Ю. Сопоставление ультразвуковых признаков, данных компьютерной томографии и морфологического исследования легких у пациентов с коронавирусной инфекцией: *post hoc* анализ. *Вестник интенсивной терапии им. А.И. Салтанова*. 2023;3:82–96. <https://doi.org/10.21320/1818-474X-2023-3-82-96>

📅 *Поступила:* 01.02.2023

📅 *Принята к печати:* 03.06.2023

📅 *Дата онлайн-публикации:* 28.07.2023

Introduction

In coronavirus infection (COVID-19), alveolar cells are the main and rapidly attainable target of the pathogen, which determines the development of pneumonia with extensive lung damage [1–5]. Therefore, scanning techniques that can detect lung lesions have gained an important role [6–8]. Computed tomography (CT) of the chest is the most informative method of diagnosing inflammatory lung disease and is crucial in visualising pathological changes in the lungs in COVID-19 [9–12]. In patients with coronavirus infection there are typical manifestations of viral pneumonia, which include “ground-glass opacity” — thickening of lung tissue of predominantly round shape, of different extent with or without consolidation, reticular changes, symptom of “cobblestone pavement”; thickening of interlobular interstitium; consolidation areas, perilobular thickening (combined with “ground-glass opacity” — thickening of pulmonary parenchyma); symptom of air bronchography [7, 11, 13, 14].

Lung ultrasound (LUS) has been an underestimated diagnostic tool for many years, as the normal air lung is a barrier to the propagation of ultrasound ultrasonic waves [15]. Initially, ultrasound was only used to diagnosis of pathological lesions in the pleural cavity (free fluid, tumour lesions) [15]. Subsequently, it was found that pulmonary tissue lesions result of reduced aeration and exposure to ultrasound results in specific artefacts [16–19]. The European Respiratory Society Consensus on Thoracic Ultrasound has stratified the ultrasound assessment of the chest wall, parietal pleura, pleural effusion, diaphragm and has characterised the ultrasound signs of pneumothorax, interstitial syndrome and lung consolidation [18]. A number of studies have investigated the relationship between CT and ultrasound signs based on correlation analysis and simple data matching [9, 13, 20–24]. However, the approaches of signs’ assessment and techniques for assessing detected by ultrasound and CT are differ between investigators [9, 19, 20, 23].

The aim of the study was to investigate the correspondence of determined ultrasound signs with those of CT scan and morphological data in patients with COVID-19 pneumonia.

Materials and methods

Protocols, statistical analysis and main results of lung ultrasound study in COVID-19 were published earlier [25]. The clinical study was performed in the Federal State Budgetary Educational Institution of Higher Professional Education “Kirov Military Medical Academy” of the Ministry of Defense of Russia. The study was approved by an independent Ethics Committee (protocol no 236, dated 21.05.2020). A total of 388 patients who un-

derwent lung ultrasound and CT scanning were included in the post hoc analysis [25].

The study was prospective. Inclusion criteria were: age of patients 18–75 years; development of community-acquired pneumonia; confirmed COVID-19 or suspected COVID-19. Inclusion criteria were: presence of pneumothorax; history of chest trauma or lung surgery; background specific diseases (tuberculosis, sarcoidosis). Bedside ultrasound was performed using a portable ultrasound machine (Mindray M7, China), with a 2.5–5 MHz convex transducer. The imaging procedure was standardised using an abdominal examination preset, with a maximum depth of 18 cm, focusing on the pleural line. Gain was adjusted to obtain the best image of the pleura, vertical artefacts and subpleural consolidations with or without air bronchograms. All harmonics and software for artifact reduction were disabled. The examination was performed in the supine or sitting position, depending on the patient’s condition. Lung ultrasound was performed according to the 16-zone Russian protocol (eight zones right and left) [26]. CT was performed on Philips Ingenuity (128 slices). The period between CT and lung ultrasound was not more than 24 h.

Morphological data were obtained from pathological examination of deceased patients. Material for histological analysis was taken in the areas of the most typical ultrasound features. Lung tissue sections fixed in formalin buffered solution were dehydrated and embedded into paraffin blocks. Serial sections of 5–6 microns in thickness were made on a rotary microtome HM 3600 (MICROM Laborgerdte GmbH, Germany), which were placed on slides. Histological sections were stained with hematoxylin and eosin and examined in the light field using an Olympus BX46 microscope.

Data collection and statistical analysis

The data for this work were obtained from the original COVID-19 lung ultrasound study [25]. Lung CT scans were used to identify pathological features, which were recorded according to lung segments. To verify bronchopulmonary segments on CT, we used numbering and anatomical nomenclature adopted by London International Congress of Otolaryngologists in 1949 and Paris International Congress of Anatomists in 1955. Lung ultrasound used projection of lung segments on “Russian protocol” zones, where pathological signs were determined and compared with CT findings. Intrasegmental spatial localization of the sign was taken into account.

Statistical analysis was performed using SPSS-26 for Windows (Statistical Package for Social Science, SPSS Inc. Chicago IL, USA). With a normal distribution the data were represented by the mean and standard deviation $M (\pm SD)$; descriptions of quantitative data that did not obey the law of normal distribution were presented as median and 25th and 75th percentiles — $Me (Q1; Q3)$. Analysis was performed to describe and summarise the distributions of the variables. The description of frequencies in the study

sample is presented with a mandatory reference to the cited sample characteristic (n (%)). Comparison of the features detected by CT and lung ultrasound was performed by multivariate correspondence analysis, by constructing a contingency table and graphically representing the rows and columns of the table as points in space. Tests were considered statistically significant at $p < 0.05$.

Results

A total of 388 patients were included in the study. Oxygen support was required in 252 (64.9%) patients. According to the degree of lung injury according to CT scanning, the patients were distributed as follows: CT-2 — 207 (53.4%); CT-3 — 156 (40.2%); CT4 — 25 (6.4%) (Table 1). Bilateral involvement was found in 100% of cases. Blood oxygen saturation (SpO_2) during self-breathing with air (for calculations, oxygen concentration in air (FiO_2))

was defined as 21%) was SpO_2 — 93 (86; 97), SpO_2/FiO_2 ratio — 380 (260; 462).

Characteristic CT signs of coronavirus pneumonia were: thickening of pulmonary parenchyma -“ground-glass opacities”, thickened pleura, consolidation, reticular thickening of interstitium, crazy-paving pattern, air bronchogram, free fluid in pleural cavity. The lung ultrasound showed signs of pleural thickening, various B-line features (multifocal, discrete or confluent), signs of consolidation (subpleural or segmental, lobular), air bronchogram, free fluid in the pleural cavity. The frequency of signs is shown in Table 2.

Comparison of features detected by CT and lung ultrasound was performed in a multivariate correspondence analysis by constructing a contingency table and graphically representing the rows and columns of the table as points in space.

The analysis was performed using a three-dimensional solution, as a jump from the fourth to the fifth axis occurred. The first three axes together explained 64.9% of the inertia, which was a good indicator of solution quality (Table 3).

Table 1. Characteristics of patients included in the study

Characteristics	Value
Age, years (M ± SD)	52.6 ± 10.5
Sex (male/female), n	267/121
Height, cm (M ± SD)	173.4 ± 12.4
Body weight, kg (M ± SD)	94.2 ± 17
Body mass index, kg/m^2 (M ± SD)	31.2 ± 4.7
Day of illness on admission to hospital (M ± SD)	5.4 ± 2.0
Moderate/severe pneumonia, n	184/204
Blood saturation (SpO_2) when breathing atmospheric air, Me (Q1; Q3)	93 (86; 97)
Number of patients with baseline decreased (< 94%) saturation when breathing atmospheric air, n (%)	252 (64.9)
Mortality, n (%)	56 (14.4)
Degree of lesion on CT scan	
2	207 (53.4)
3	156 (40.2)
4	25 (6.4)
Concomitant diseases, n (%)	
Diabetes mellitus	78 (20.1)
Obesity	193 (49.7)
Hypertension	252 (64.9)
Coronary heart disease	95 (24.5)
Chronic heart failure	20 (5.1)

Table 2. Frequency of detection of signs according to CT and lung ultrasound

The study	Code of sign	Sign	n (%)
Lung CT	1	Thickened pleura	310 (79.9)
	2	Thickening of pulmonary parenchyma — "ground-glass opacities"	388 (100)
	3	Reticular thickening of interstitium	115 (29.6)
	4	Subpleural consolidation	144 (37.1)
	5	Segmental (lobular) consolidation	174 (44.8)
	6	Air bronchogram with signs of consolidation	132 (34.0)
	7	Symptom of "cobblestone pavement"	48 (12.4)
	8	Free fluid in pleural cavity.	43 (11.1)
Lung US sign	10	B-lines (multifocal, discrete or confluent)	388 (100)
	11	Pleural line thickening	321 (82.7)
	12	Subpleural consolidation	174 (44.8)
	13	Segmental (lobular) consolidation	182 (46.9)
	14	Air bronchogram	143 (36.9)
	15	Free fluid in pleural cavity	54 (13.9)

In a graphical mapping of the correlation between CT and ultrasound findings, three features are identified as separate from the main dataset. These are a thickened pleura, an air bronchogram and free fluid in the pleural cavity. It should be noted that the distances between the CT and ultrasound findings are short, further emphasising the conjugation of features in the correlation table (Figure 1).

The data set characterising pulmonary tissue infiltration and consolidation changes included B-lines, subpleural, segmental and lobular consolidation traits, reticular changes and cobblestone pavement traits were concentrated in one area of the map; there was overlap of points on the matching map (Figure 3), which made interpretation of the data difficult, so coordinate points should be used to estimate

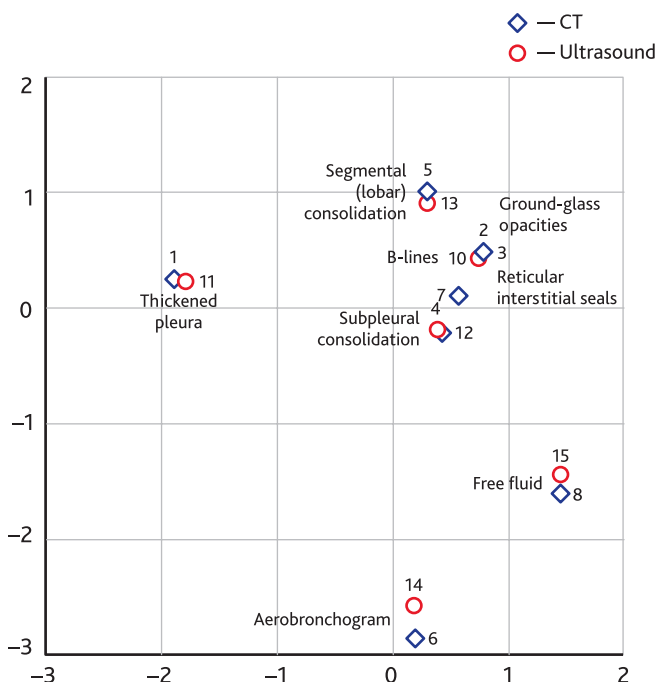


Fig. 1. Map of the correspondence of signs of CT and lungs ultrasound

Coding of CT signs: 1 — thickened pleura; 2 — compaction of the pulmonary parenchyma by the type of "ground-glass opacity"; 3 — reticular interstitial seals; 4 — subpleural consolidation; 5 — segmental (lobar) consolidation; 6 — airbronchogram; 7 — symptom of "cobblestone pavement"; 8 — free fluid in the pleural cavity. Coding of lung ultrasound signs: 10 — B-lines; 11 — thickened pleura; 12 — subpleural consolidation; 13 — segmental (lobar) consolidation; 14 — airbronchogram; 15 — free fluid in the pleural cavity.

Table 3. Singular values, inertia and fractions of inertia

Measurement	Singular value	Inertia	χ^2	p	Share of inertia	
					Taken into account	Total
1	0.954	0.911	—	—	0.229	0.229
2	0.929	0.863	—	—	0.217	0.447
3	0.896	0.803	—	—	0.202	0.649
4	0.869	0.755	—	—	0.190	0.839
5	0.799	0.639	—	—	0.161	1.000
Total	—	3.971	5821.199	0.00	1.000	1.000

the distance between the points belonging to the CT and ultrasound lung traits (Table 4).

Immediately adjacent to the CT signs of “ground-glass opacities” and reticular thickening is the ultrasound sign of B-lines. Next to the CT sign of subpleural consolidation is the ultrasound sign with the same name, as well as the CT and ultrasound signs of segmental (lobular) consolidation. CT sign “cobblestone pavement” is located between the ultrasound signs of subpleural consolidation and B-lines.

A table based on the pairing showed the concordance between the features of lung ultrasound and CT scan-

ning (Table 5). If pleural thickening was detected on CT, then a thickened pleural line was also visualized on ultrasound. The most common CT findings were “ground-glass opacities” — thickening of the pulmonary parenchyma, with B-lines (multifocal, discrete or confluent) corresponding to this on LUS. If reticular thickening of the interstitium reached the pleura or consolidation zone, it was identified as B-line (more often discrete) on ultrasound. CT signs of subpleural and segmental (lobular) consolidation corresponded to ultrasound signs of subpleural and segmental (lobular) consolidation. While the CT scan

Table 4. Coordinate points of signs of CT and lung ultrasound

Research	Sign	Mass	Estimates in measurement			Inertia
			1 axis	2 axis	3 axis	
Lung US	B-lines	0.381	0.739	-0.702	0.439	0.514
	Thickened pleura	0.218	-1.806	-0.288	0.227	0.709
	Subpleural consolidation	0.15	0.375	-0.109	-0.195	0.551
	Segmental (lobular) consolidation	0.12	0.276	2.407	0.907	0.751
	Air brochogram	0.098	0.181	0.46	-2.559	0.714
	Free fluid	0.033	0.169	0.395	-1.439	0.732
CT	Thickened pleura	0.2	-1.893	-0.31	0.254	0.716
	“Ground-glass opacities”	0.255	0.774	-0.755	0.49	0.414
	Reticular thickening	0.065	0.774	-0.755	0.49	0.106
	Subpleural consolidation	0.074	0.393	-0.117	-0.218	0.421
	Segmental (lobular) consolidation	0.102	0.289	2.591	1.012	0.75
	Air brochogram	0.076	0.19	0.495	-2.856	0.701
	Symptom of “cobblestone pavement”	0.065	0.569	-0.413	0.11	0.096
	Free fluid	0.025	0.177	0.425	-1.606	0.725

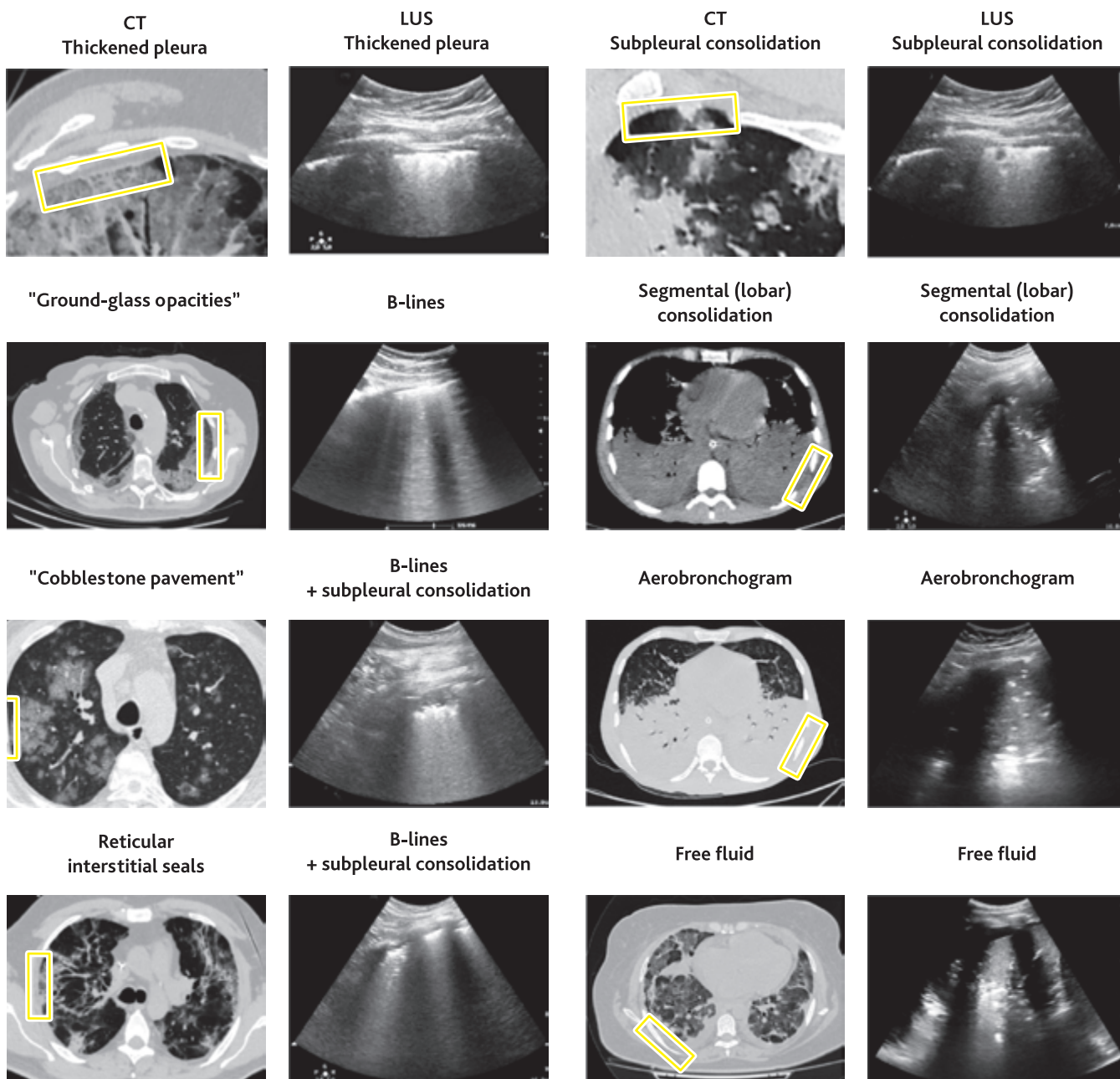


Fig. 2. Correspondence of signs of CT and lung ultrasound

showed air bronchi in the background of the consolidation sign, the ultrasound scan visualized air bronchogram within the consolidation zones, which was usually dynamic in nature. The “cobblestone pavement” symptom on CT was due to a combination of “ground-glass opacities” sign and thickened interlobular septa, this combination was characterised by a combination of B-lines interspersed with small subpleural consolidation in areas of septal thickening and alveolar lesions on LUS. Free fluid in the pleural cavity was rarely detected and was associated with severe, prolonged disease, accession of bacterial microflora and decompensated heart failure. A visual correlation be-

tween CT and ultrasound findings in the lungs is shown in Figure 2.

A comparison of lung ultrasound signs and histological findings was performed in 6 patients who died on 2, 3, 5, 8, 12, 18 days. Autopsy material for histological examination was taken from the subpleural area with a section of the pleura. The analysis showed that ultrasound signs could be caused by different pathomorphological manifestations.

The ultrasound sign of B-lines corresponded histologically to manifestations of diffuse alveolar damage in the exudative and proliferative phases. In the exudative phase

Table 5. Table of correspondences of signs of CT and lung ultrasound

CT	Sign	Lung US						
		B-lines	Thickened pleura	Subpleural consolidation	Segmental (lobular) consolidation	Air brochoqram	Free fluid	Active field
	Thickened pleura	0	293	0	0	0	0	293
	"Ground-glass opacities"	374	0	0	0	0	0	374
	Reticular thickening	96	0	0	0	0	0	96
	Subpleural consolidation	0	0	109	0	0	0	109
	Segmental (lobular) consolidation	0	0	0	150	0	0	150
	Air brochoqram	0	0	0	0	111	0	111
	Symptom of "cobblestone pavement"	44	0	51	0	0	0	95
	Free fluid	0	0	0	0	0	36	36
	Active field	559	320	220	176	143	48	1466

B-lines were caused by exudation of fluid and protein molecules into the intra-alveolar space against the background of massive death of type 1 alveolocytes and capillary endothelium damage leading to infiltration of serous exudate into the alveolar lumen with attachment of precipitates and fibrin threads (Figure 3, *B*). A perivascular inflammatory-cellular reaction was detected in all deceased patients. It included clusters of lymphoid cells and macrophages. In severe endothelial damage, the appearance of erythrocytes in the interstitium and inside the alveoli was observed (Figure 3, *A*). At treatment duration of more than 3–5 days there were signs of early proliferative phase characterized by the progression of diffuse alveolar damage with the development of intraalveolar edema (Figure 3, *B*), as well as the formation of hyaline membranes. Macrophages, desquamated alveolar epithelial cells, lymphoid cells and polymorphonuclear leukocytes were detected in the alveolar lumen (Figure 3, *D*). In 100% of cases interalveolar septa were deformed and thickened due to edema on the background of inflammatory-cellular infiltration represented by macrophages, lymphoid cells, polymorphonuclear leukocytes (Figure 3, *D*). In addition, signs of microcirculatory disorders in the form of erythrocyte sludge, stasis, foci of extravasation and dilatation of capillaries were determined in all cases. Fibrin and erythrocyte-fibrin thrombi were detected in the lumen of pulmonary arterioles branches. Endothelium in the areas of thrombotic masses attachment was characterized by enlarged nuclei, signs of intracellular edema and swelling (Figure 3, *A, E*).

Ultrasound evidence of consolidation appears in the airless zone of the lung. The size of the consolidated zones

varied from a few millimetres to consolidation of the entire lobe. Small areas of subpleural consolidation were due to thickening and inflammatory lympho-leucocytic infiltration of the pleura, as well as the development of subpleural haemorrhages, diffuse alveolar damage, with death and recession of alveolocytes, perivascular inflammatory-cellular reaction due to accumulation of lymphoid cells and macrophages (Figure 4, *A, B*). Large volumes of consolidation in the exudative phase were formed due to intra-alveolar edema, layering of desquamated alveolar epithelium and macrophages in the alveolar lumen (Figure 4, *D*). Progression of the pathology into the proliferative phase was characterized by the formation of band-like homogeneous eosinophilic masses, so-called hyaline membranes, along the contours of alveolar passages, alveolar sacs, alveoli and some bronchioles with a decrease in airiness of lung tissue. Also denudation of basal membranes of aerohematic barrier with destruction of its "working zone" and presence of diffusely located cellular infiltrates from pulmonary macrophages, polymorphonuclear leukocytes, few lymphocytes in alveoli lumen among fragmented hyaline membranes was typical (Figure 4, *E*). During treatment for more than 7 days, the lung tissue showed signs of disorganization of the organ structure due to the developing fibrosis. Histologically, on the background of diffuse pulmonary infiltration with macrophages, polymorphonuclear leukocytes and few lymphocytes due to fibroblast proliferation and increased volume of collagen fibers, there was thickening of interalveolar septa with reduction of their capillary channel and collapsing alveoli (Figure 4, *F*).

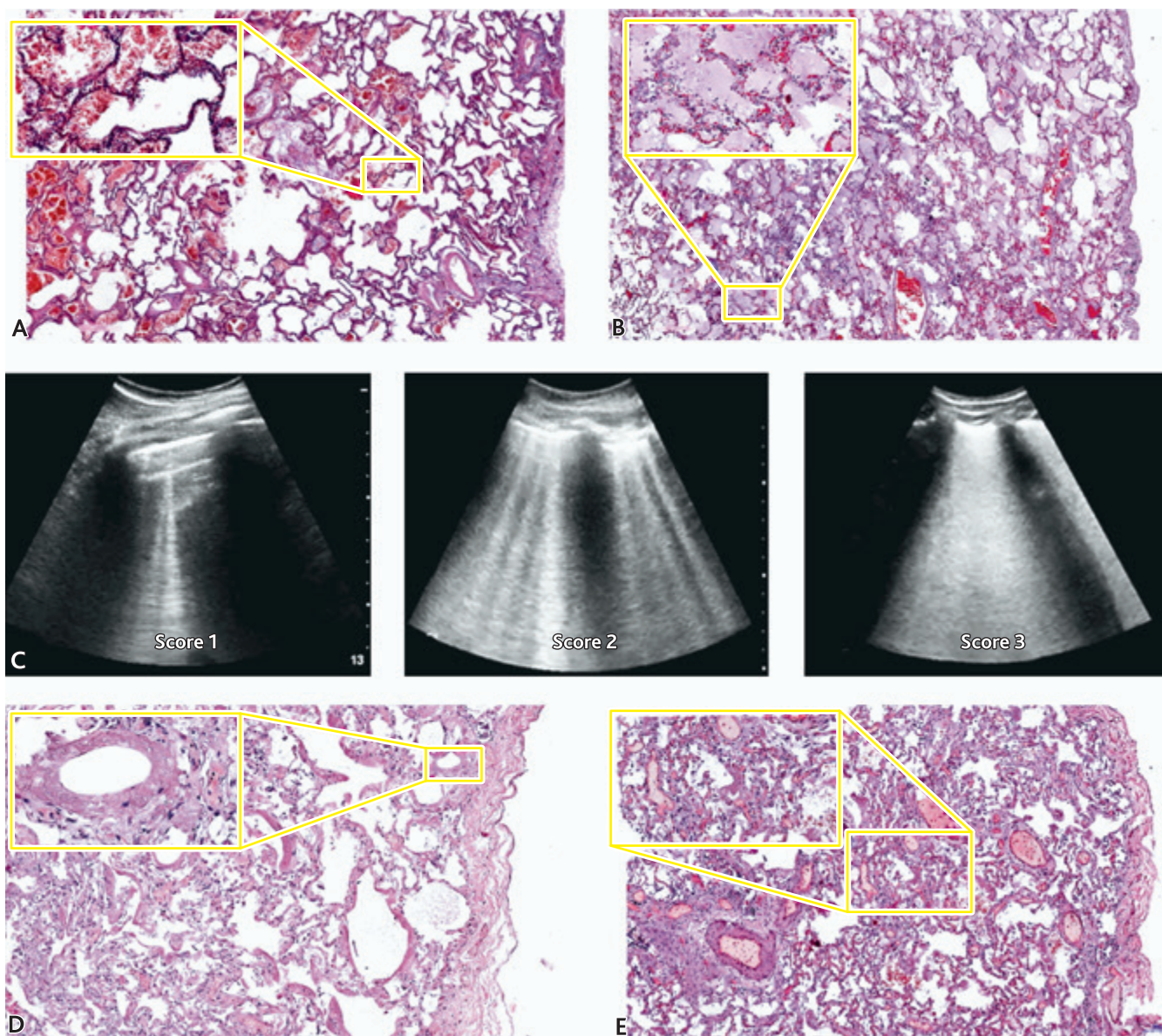


Fig. 3. Comparison of the feature of B-lines and histological data:

A — zones of atelectatic and emphysematous changes. Intraalveolar focal hemorrhages; *B* — a decrease in the airiness of the lung due to intraalveolar edema, overstretching and rupture of the interalveolar septa, fullness of the vessels of the microcirculatory bed — pulmonary edema; *C* — the degree of severity of the ultrasound of the B-line sign in points according to the "Russian Protocol"; *D* — reduction of lung airiness due to thickening and deformation of the interalveolar septa due to their inflammatory infiltration. Homogeneous eosinophilic protein overlays — hyaline membranes in the lumen of the alveoli; *E* — decrease in the airiness of the lung due to the collapse of the alveoli. In the lumen of the alveoli desquamated alveolocytes and macrophages. Thrombosis of vessels of medium and small caliber.

Discussion

Lung ultrasound has been studied in a number of studies and is included in diagnostic protocols for coronavirus infection [27–29]. In the diagnosis of pneumonia, lung ultrasound can achieve 75–90% specificity and 65–95% sensitivity [30–33]. Ultrasound has been shown to have higher sensitivity, specificity and accuracy for the diagnosis of lung lesions compared with chest radiography [34, 35]. In the Cochrane

systematic review, the sensitivity of CT in the diagnosis of COVID-19 lung lesions was 86.9% (95% confidence interval [CI] 83.6; 89.6) and the specificity 78.3% (95% CI 73.7; 82.3). For chest radiography, the sensitivity for chest radiography was 73.1% (95% CI 64; 80.5) and the specificity 73.3% (95% CI 61.9; 82.2). For lung ultrasound, the sensitivity was 88.9% (95% CI 84.9; 92.0) and the specificity 72.2% (95% CI 58.8; 82.5). This study demonstrated that chest CT scan and lung ultrasound are sensitive

and moderately specific for the diagnosis of COVID-19, and chest radiography is inferior to them in terms of sensitivity of the method in the diagnosis of COVID-19 lung tissue lesions [36].

As in our work, the most common CT signs of pulmonary involvement in COVID-19 in other studies were “frosted glass” infiltration with or without consolidation. The “frosted glass” sign was predominantly bilateral,

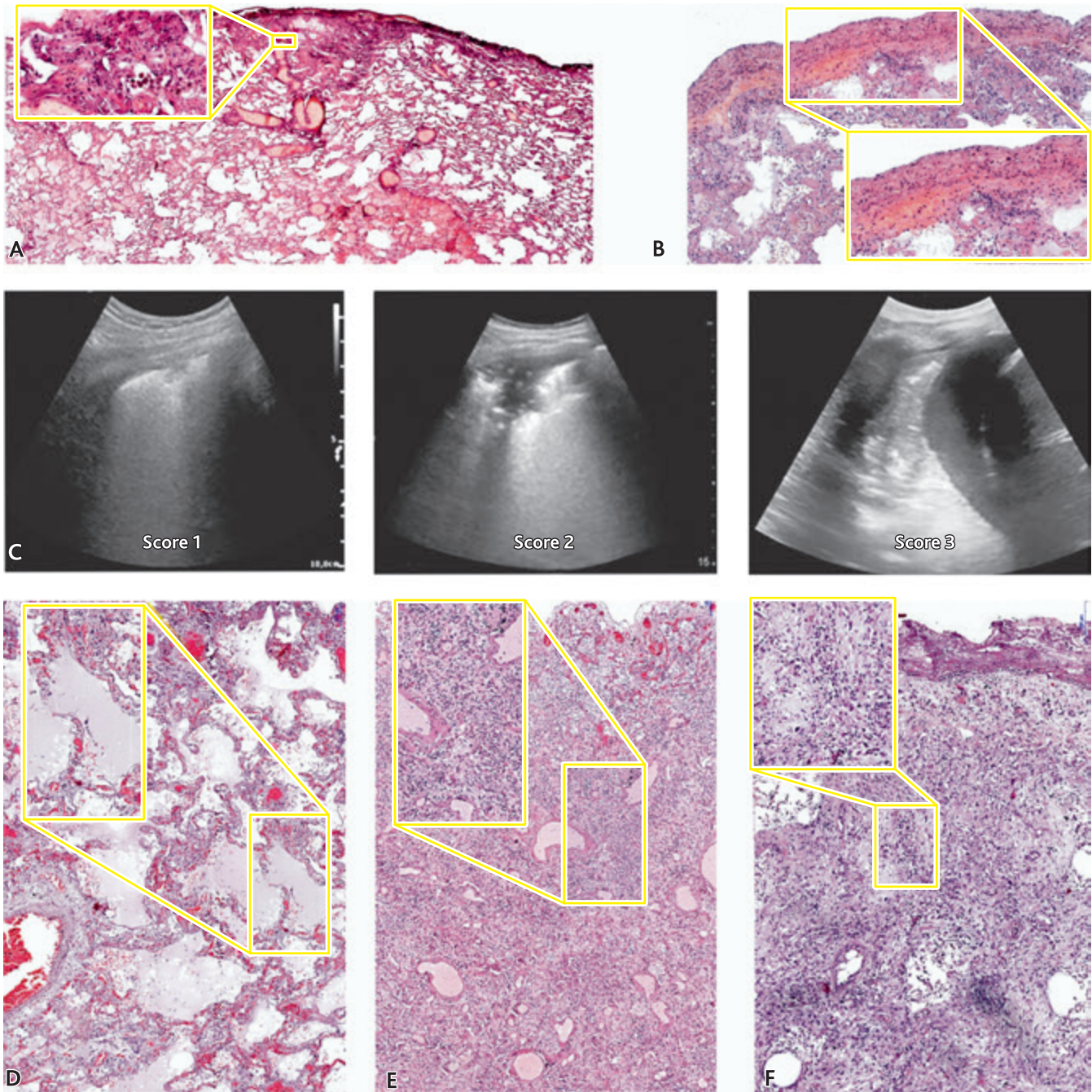


Fig. 4. Comparison of consolidation sign and histological data:

A — subpleural consolidation. Foci of the forming connective tissue next to the thrombosed vessel. Focal accumulations of edematous fluid in the alveolar cavities; *B* — subpleural hemorrhage, collapse of the alveoli with hyaline membranes and leukocyte infiltration. Areas of emphysematous enlargement and atelectasis of the lung; *C* — the degree of severity of the consolidation sign in points according to the “Russian Protocol”; *D* — alveoli with edematous fluid containing exfoliated alveolocytes and neutrophils. Fullness of the vessels of the interalveolar septa; *E* — deformation and change of histoarchitecture of the lung due to the growth of connective tissue in it; *F* — formation of mature connective tissue in the lung parenchyma and visceral pleural leaf.

peripheral, multifocal. The consolidation sign was mostly bilateral with predominantly subpleural peripheral location and/or consolidation of the whole segment (lobe). Additional CT signs were cobblestone pavement pattern, pleural thickening, air bronchogram sign, reticular changes. Pleural effusion was infrequent and mostly small [37–40].

The sonographic features of COVID-19 were similar to those of other types of viral pneumonia [16, 41–44]. In most studies, the main sonographic sign observed in patients with COVID-19 was B-lines [18, 19, 28, 32, 45–47]. There are many varieties of B-lines, such as single, focal, which appear in small lesions, multifocal single or confluent up to “white lung” B-lines, occurring with increasing volume and severity of lung tissue changes [18, 19, 35, 48, 49]. In a cohort of 105 patients with COVID-19, 92 % of patients had confluent B-lines and 38 % had the feature of “white lung” [50]. Another sonographic sign, found in 70 % of cases according to the literature [48], was a small subpleural consolidation [49]. More extensive subpleural thickening in the posterolateral regions was usually seen in ventilated patients and could be accompanied by air bronchograms [49–52]. Changes to the pleural line in COVID-19 were frequently visualised. The pleural line was thickened, irregular or fragmented in affected areas [35, 46].

We did not find multivariate analysis of the correspondence between ultrasound and CT signs in the literature. Current studies have been limited to simple comparisons of data and examination of correlations between features. All studies showed correlation between CT and ultrasound findings. The strength of the correlation was assessed as moderate [48] or strong [9, 53]. In our study, there were statistically proven correspondences between signs of “ground-glass opacities” — lung parenchyma thickening and B-lines, different consolidation volumes, air bronchogram, pleural and pleural line changes, free fluid in pleural cavity. The same correspondence was found by other researchers [9, 20, 48, 49, 54].

Diffuse alveolar damage is the main histological finding in morphological studies of the lungs of patients with coronavirus infection [55–57]. During progression, diffuse alveolar damage undergoes an exudative phase, an early and late proliferative or organising phase and a late fibrous phase [58, 59]. The exudative and proliferative phases have the greatest impact on the alveolar and interstitial space, forming the basis for ultrasound artifacts [17, 57]. Cell death with loss of epithelial layer inside alveoli, capillary endothelium damage leads to increase of extravascular fluid up to intra-alveolar hemorrhage [59, 60]. Hyaline membranes appear early in the disease and interstitial and alveolar oedema increase. In addition, thrombosis of the affected capillaries, haemorrhage, infiltration with inflammatory cells, scattered fibroblasts, thickening of the alveolar septa, denudation of the alveolar epithelium and type II hyperplasia develop. The proliferation phase is characterised by proliferation of fibroblasts in the septa and alveolar spaces and the appearance of atypical pneumocytes against a background of still impaired microcirculation. The organization phase can move

to the fibrous stage after about 3–4 weeks [55–59]. Our work has shown that ultrasound signs of B-lines and consolidation can be detected in the exudative, proliferative and fibrotic stages and depend on the airiness of the alveoli. We found only one study in the form of a letter to the editor which compared lung ultrasound findings with histological findings [61]. In the work of A. Monteiro et al. (2020) reported that COVID-19 pneumonia on early-stage lung ultrasound was characterised with an irregular and thickened pleural line with demonstration of B-lines and areas of air lung. These features were consistent with acute diffuse lung damage with hyaline membranes. The interstitial phase on ultrasound was characterised by pleural thickening with subpleural thickening, which morphologically corresponded to early fibroproliferative changes associated with acute diffuse alveolar damage. Large areas of consolidation were histologically associated with fibroproliferative changes and loss of alveolar airiness on ultrasound [61].

The strength of our work was the ultrasound of 16 areas of the chest compared to other studies that have used protocols with 14, 12, 8, 6 areas assessed, as scanning fewer lung areas can impair diagnostic accuracy [32].

Study limitations

The present study had some limitations. Firstly, it was a post hoc analysis of a prospective observational study with no randomisation or blinding design. Secondly, there was a gender bias towards men, due to the nature of the medical organisation where the study was conducted.

Conclusion

CT is the gold standard for assessing the extent and nature of lung damage in patients with COVID-19. Multivariate correlation analysis showed a correlation between CT and ultrasound findings in the lungs. CT signs of “ground-glass opacities” corresponded to B lines in ultrasound; CT signs of consolidation corresponded to ultrasound signs of consolidation; air bronchogram CT signs to air bronchogram ultrasound; free fluid CT signs to free fluid ultrasound. CT signs of reticular changes and symptom of “cobblestone pavement” corresponded to different combinations of ultrasound signs of subpleural consolidation and B-lines. Morphological analysis showed polymorphic histological findings, leading to ultrasound signs. The diagnostic methods used do not replace each other, but complement each other, which contributes to a better assessment of changes in the lungs and can influence the change in treatment tactics.

Disclosure. The authors declare that they have no competing interests.

Author contribution. All authors according to the ICMJE criteria participated in the development of the concept of the article, obtaining and analyzing factual data, writing

and editing the text of the article, checking and approving the text of the article.

Ethics approval. This study was approved by the independent Ethical Committee of Military Medical Academy, St. Petersburg, Russia (reference number: 236-21.05.2020).

Author's ORCID:

Lakhin R.E. — 0000-0001-6819-9691

Zhirnova E.A. — 0000-0003-1865-3838

Shchegolev A.V. — 0000-0001-6431-439X

Funding source. This study was not supported by any external sources of funding.

Data Availability Statement. The data that support the findings of this study are openly available in repository Mendeley Data at <http://doi.org/10.17632/zjhjmrz4vh.1>

Zheleznyak I.S. — 0000-0001-7383-512X

Chirsky V.S. — 0000-0002-8336-1981

Pluminsky D.Y. — 0000-0003-0368-4260

References

- [1] Seyed Hosseini E., Riahi Kashani N., Nikzad H., et al. The novel coronavirus Disease-2019 (COVID-19): Mechanism of action, detection and recent therapeutic strategies. *Virology*. 2020; 551: 1–9. DOI: 10.1016/j.virol.2020.08.011
- [2] Sharma A., Ahmad Farouk I., Lal S.K. COVID-19: A Review on the Novel Coronavirus Disease Evolution, Transmission, Detection, Control and Prevention. *Viruses*. 2021; 13(2). DOI: 10.3390/v13020202
- [3] Umakanthan S., Sahu P., Ranade A.V., et al. Origin, transmission, diagnosis and management of coronavirus disease 2019 (COVID-19). *Postgrad Med J*. 2020; 96(1142): 753–8. DOI: 10.1136/postgradmedj-2020-138234
- [4] Avdeev S.N., Nekludova G.V., Trushenko N.V., et al. Lung ultrasound can predict response to the prone position in awake non-intubated patients with COVID-19 associated acute respiratory distress syndrome. *Crit Care*. 2021; 25(1): 35. DOI: 10.1186/s13054-021-03472-1
- [5] Rothe C., Schunk M., Sothmann P., et al. Transmission of 2019-nCoV Infection from an Asymptomatic Contact in Germany. *N Engl J Med*. 2020; 382(10): 970–1. DOI: 10.1056/nejmc2001468
- [6] Chung M., Bernheim A., Mei X., et al. CT imaging features of 2019 novel coronavirus (2019-nCoV). *Radiology*. 2020; 295(1): 202–7. DOI: 10.1148/radiol.2020200230
- [7] Xu X., Yu C., Qu J., et al. Imaging and clinical features of patients with 2019 novel coronavirus SARS-CoV-2. *Eur J Nucl Med Mol Imaging*. 2020; 47(5): 1275–80. DOI: 10.1007/S00259-020-04735-9
- [8] Huang P., Liu T., Huang L., et al. Use of Chest CT in Combination with Negative RT-PCR Assay for the 2019 Novel Coronavirus but High Clinical Suspicion. *Radiology*. 2020; 295(1): 22–3. DOI: 10.1148/radiol.2020200330
- [9] Tung-Chen Y., Martí de Gracia M., Díez-Tascón A., et al. Correlation between Chest Computed Tomography and Lung Ultrasonography in Patients with Coronavirus Disease 2019 (COVID-19). *Ultrasound Med Biol*. 2020; 46(11): 2918–926. DOI: 10.1016/j.ultrasmedbio.2020.07.003
- [10] Garin N., Marti C., Scheffler M., et al. Computed tomography scan contribution to the diagnosis of community-acquired pneumonia. *Curr Opin Pulm Med*. 2019; 25(3): 242–8. DOI: 10.1097/MCP.0000000000000567
- [11] Cellina M., Orsi M., Valenti Pittino C., et al. Chest computed tomography findings of COVID-19 pneumonia: pictorial essay with literature review. *Jpn J Radiol*. 2020; 38(11): 1012–9. DOI: 10.1007/S11604-020-01010-7
- [12] Franquet T. Imaging of Community-acquired Pneumonia. *J Thorac Imaging*. 2018; 33(5): 282–94. DOI: 10.1097/RTI.0000000000000347
- [13] Nounne A., Zani M.D., Milanese G., et al. Lung Ultrasound in COVID-19 Pneumonia: Correlations with Chest CT on Hospital admission. *Respiration*. 2020; 99(7): 617–24. DOI: 10.1159/000509223
- [14] Nasir N., Habib K., Khanum I., et al. Clinical characteristics and outcomes of COVID-19: Experience at a major tertiary care center in Pakistan. *J Infect Dev Ctries*. 2021; 15(4): 480–9. DOI: 10.3855/jidc.14345
- [15] Mayo P.H., Copetti R., Feller-Kopman D., et al. Thoracic ultrasonography: a narrative review. *Intensive Care Med*. 2019; 45(9): 1200–11. DOI: 10.1007/S00134-019-05725-8
- [16] Lichtenstein D.A., Mezière G.A. Relevance of lung ultrasound in the diagnosis of acute respiratory failure the BLUE protocol. *Chest*. 2008; 134(1): 117–25. DOI: 10.1378/chest.07-2800
- [17] McElyea C., Do C., Killu K. Lung ultrasound artifacts in COVID-19 patients. *J Ultrasound*. 2022; 25(2): 333–8. DOI: 10.1007/s40477-020-00526-y
- [18] Laursen C.B., Clive A., Hallifax R., et al. European Respiratory Society Statement on Thoracic Ultrasound. *Eur Respir J*. 2020; 57(3): 2001519. DOI: 10.1183/13993003.01519-2020
- [19] Soldati G., Smargiassi A., Inchingolo R., et al. Proposal for International Standardization of the Use of Lung Ultrasound for Patients With COVID-19. *J Ultrasound Med*. 2020; 39(7): 1413–9. DOI: 10.1002/jum.15285
- [20] Ökmen K., Yıldız D.K., Soyaslan E. Comparison of lung ultrasonography findings with chest computed tomography results in coronavirus (COVID-19) pneumonia. *J Med Ultrason*. Published online 2021. DOI: 10.1007/s10396-021-01081-7
- [21] Karacaer C., Karabay O., Gunduz Y., et al. Correlation of lung ultrasound and computed tomography findings in COVID-19 pneumonia. *J Coll*

- Physicians Surg Pakistan. 2021; 30(10): S147–S152. DOI: 10.29271/jcpsp.2020.Supp2.S147
- [22] Peng Q.Y., Wang X.T., Zhang L.N. Findings of lung ultrasonography of novel corona virus pneumonia during the 2019–2020 epidemic. *Intensive Care Med.* 2020; 46(5): 849–50. DOI: 10.1007/s00134-020-05996-6
- [23] Rizzetto F., Perillo N., Artioli D., et al. Correlation between lung ultrasound and chest CT patterns with estimation of pulmonary burden in COVID-19 patients. *Eur J Radiol.* 2021; 138: 109650. DOI: 10.1016/j.ejrad.2021.109650
- [24] Trias-Sabrià P., Dorca Duch E., Molina-Molina M., et al. Radio-Histological Correlation of Lung Features in Severe COVID-19 Through CT-Scan and Lung Ultrasound Evaluation. *Front Med (Lausanne).* 2022; 9: 820661. DOI: 10.3389/fmed.2022.820661
- [25] Лакхин Р.Е., Журнова Е.А., Щеголев А.В. и др. Ультразвуковой индекс поражения легких как предиктор исходов лечения: когортное исследование 388 пациентов с коронавирусной инфекцией. *Вестник интенсивной терапии им. А.И. Салтанова.* 2022; (3): 45–56. DOI: 10.21320/1818-474X-2022-3-45-56 [Lakhin R.E., Zhirnova E.A., Shchegolev A.V., et al. Ultrasound-guided lung lesion index as a predictor of treatment outcomes: cohort study of 388 patients with coronavirus infection. *Annals of Critical Care.* 2022; 3: 45–56. DOI: 10.21320/1818-474X-2022-3-45-56 (In Russ)]
- [26] Лакхин Р.Е., Журнова Е.А. Способ фокусированного ультразвукового исследования легких (Русский протокол). Усовершенствование способов и аппаратуры, применяемых в учебном процессе, медико-биологических исследованиях и клинической практике. Под общей ред. проф. Б.Н. Котива. СПб.: ВМЕДА, 2021: 58–9. [Lakhin R.E., Zhirnova E.A. Sposob fokusirovannogo ultrazvukovogo issledovaniya legkih (Russkij protokol). Usovershenstvovanie sposobov i apparatury, primenyayemyh v uchebnom processe, mediko-biologicheskikh issledovaniyah i klinicheskoy praktike. Pod obshchey red. prof. B.N. Kotiva. SPb.: VMedA, 2021: 58–9. (In Russ)]
- [27] Allinovi M., Parise A., Giacalone M., et al. Lung Ultrasound May Support Diagnosis and Monitoring of COVID-19 Pneumonia. *Ultrasound Med Biol.* 2020; 46(11): 2908–17. DOI: 10.1016/j.ultrasmedbio.2020.07.018
- [28] McDermott C., Łacki M., Sainsbury B., et al. Sonographic Diagnosis of COVID-19: A Review of Image Processing for Lung Ultrasound. *Front big data.* 2021; 4: 612561. DOI: 10.3389/fdata.2021.612561
- [29] Manivel V., Lesnewski A., Shamim S., et al. CLUE: COVID-19 lung ultrasound in emergency department. *EMA — Emerg Med Australas.* 2020; 32(4): 694–6. DOI: 10.1111/1742-6723.13546
- [30] Barbieri G., Gargani L., Lepri V., et al. Long-term lung ultrasound follow-up in patients after COVID-19 pneumonia hospitalization: A prospective comparative study with chest computed tomography. *Eur J Intern Med.* Published online December 2022. DOI: 10.1016/j.ejim.2022.12.002
- [31] Binkiewicz-Orluk M., Konopka M., Jakubiak A., et al. Lung Ultrasonography and Computed Tomography Comparison in Convalescent Athletes after Sars-CoV-2 Infection — A Preliminary Study. *J Ultrason.* 2022; 22(90): e153. DOI: 10.15557/jou.2022.0025
- [32] Jari R., Alfuraih A.M., McLaughlan J.R. The diagnostic performance of lung ultrasound for detecting COVID-19 in emergency departments: A systematic review and meta-analysis. *J Clin Ultrasound.* 2022; 50(5): 618–27. DOI: 10.1002/jcu.23184
- [33] Sorlini C., Femia M., Nattino G., et al. The role of lung ultrasound as a frontline diagnostic tool in the era of COVID-19 outbreak. *Intern Emerg Med.* 2021; 16(3): 749–56. DOI: 10.1007/s11739-020-02524-8
- [34] Dhawan J., Singh G. Bedside Lung Ultrasound as an Independent Tool to Diagnose Pneumonia in Comparison to Chest X-ray: An Observational Prospective Study from Intensive Care Units. *Indian J Crit Care Med.* 2022; 26(8): 920. DOI: 10.5005/jp-journals-10071-24283
- [35] Caroselli C., Blaivas M., Marcosignori M., et al. Early Lung Ultrasound Findings in Patients With COVID-19 Pneumonia: A Retrospective Multicenter Study of 479 Patients. *J Ultrasound Med.* 2022; 41(10): 2547–56. DOI: 10.1002/jum.15944
- [36] Islam N., Ebrahimzadeh S., Salameh J.P., et al. Thoracic imaging tests for the diagnosis of COVID-19. *Cochrane database Syst Rev.* 2021; 3(3). DOI: 10.1002/14651858.CD013639.PUB4
- [37] Roberto G., Roberta F., Paola B.M., et al. Coronavirus disease 2019 (COVID-19) in Italy: features on chest computed tomography using a structured report system. *Sci Rep.* 2020; 10(1). DOI: 10.1038/S41598-020-73788-5
- [38] Zhou X., Pu Y., Zhang D., et al. CT findings and dynamic imaging changes of COVID-19 in 2908 patients: a systematic review and meta-analysis. *Acta Radiol.* 2022; 63(3): 291–310. DOI: 10.1177/0284185121992655
- [39] Zarifian A., Ghasemi Nour M., Akhavan Rezayat A., et al. Chest CT findings of coronavirus disease 2019 (COVID-19): A comprehensive meta-analysis of 9907 confirmed patients. *Clin Imaging.* 2021; 70: 101–10. DOI: 10.1016/j.clinimag.2020.10.035
- [40] Garg M., Gupta P., Maralakunte M., et al. Diagnostic accuracy of CT and radiographic findings for novel coronavirus 2019 pneumonia: Systematic review and meta-analysis. *Clin Imaging.* 2021; 72: 75–82. DOI: 10.1016/j.clinimag.2020.11.021
- [41] Li L., Qin A., Yang X., et al. Findings and Prognostic Value of Lung Ultrasonography in Coronal Virus Disease 2019 (COVID-19) Pneumonia. *Shock.* 2021; 56(2): 200–5. DOI: 10.1097/SHK.0000000000001700
- [42] Recinella G., Marasco G., Tufoni M., et al. Clinical Role of Lung Ultrasound for the Diagnosis and Prognosis of Coronavirus Disease Pneumonia in Elderly Patients: A Pivotal Study. *Gerontology.* 2021; 67(1): 78–86. DOI: 10.1159/000512209
- [43] Cho Y.J., Song K.H., Lee Y., et al. Lung ultrasound for early diagnosis and severity assessment of pneumonia in patients with coronavirus disease 2019. *Korean J Intern Med.* 2020; 35(4): 771–81. DOI: 10.3904/kjim.2020.180
- [44] Chavez M.A., Shams N., Ellington L.E., et al. Lung ultrasound for the diagnosis of pneumonia in adults: a systematic review and meta-analysis. *Respir Res.* 2014; 15: 50. DOI: 10.1186/1465-9921-15-50
- [45] Sultan L.R., Sehgal C.M. A Review of Early Experience in Lung Ultrasound in the Diagnosis and Management of COVID-19. *Ultrasound Med Biol.* 2020; 46(9): 2530–45. DOI: 10.1016/j.ultrasmedbio.2020.05.012
- [46] Mohamed M.F.H., Al-Shokri S., Yousaf Z., et al. Frequency of Abnormalities Detected by Point-of-Care Lung Ultrasound in Symptomatic COVID-19 Patients: Systematic Review and Meta-Analysis. *Am J Trop Med Hyg.* 2020; 103(2): 815–21. DOI: 10.4269/ajtmh.20-0371
- [47] Мишина Е.А., Иванова И.В., Пыхова А.Ю. и др. Ультразвуковое исследование легких в условиях реанимационного отделения пе-

- ринатального центра. Анестезиология и реаниматология. 2022; (5): 67–70. DOI: 10.17116/anaesthesiology202205167 [Mishina E.A., Ivanova I.V., Pykhova A.Y., et al. Lung ultrasound in the intensive care unit of the perinatal centre. Russ J Anesthesiol Reanimatol. Anesteziologiya i Reanimatol. 2022; 2022(5): 67–70. DOI: 10.17116/anaesthesiology202205167 (In Russ)]
- [48] Ciurba B.E., Sárközi H.K., Szabó I.A., et al. Applicability of lung ultrasound in the assessment of COVID-19 pneumonia: Diagnostic accuracy and clinical correlations. *Respir Investig.* 2022; 60(6): 762–71. DOI: 10.1016/j.resinv.2022.06.015
- [49] Gil-Rodríguez J., Pérez de Rojas J., Aranda-Laserna P., et al. Ultrasound findings of lung ultrasonography in COVID-19: A systematic review. *Eur J Radiol.* 2022; 148. DOI: 10.1016/j.ejrad.2022.110156
- [50] Yasukawa K., Minami T., Boulware D.R., et al. Point-of-Care Lung Ultrasound for COVID-19: Findings and Prognostic Implications From 105 Consecutive Patients. *J Intensive Care Med.* 2021; 36(3): 334–42. DOI: 10.1177/0885066620988831
- [51] Seiler C., Klingberg C., Hårdstedt M. Lung Ultrasound for Identification of Patients Requiring Invasive Mechanical Ventilation in COVID-19. *J Ultrasound Med.* 2021; 40(11): 2339–51. DOI: 10.1002/jum.15617
- [52] Xing C., Li Q., Du H., et al. Lung ultrasound findings in patients with COVID-19 pneumonia. *Crit Care.* 2020; 24(1). DOI: 10.1186/s13054-020-02876-9
- [53] Giovannetti G., De Michele L., De Ceglie M., et al. Lung ultrasonography for long-term follow-up of COVID-19 survivors compared to chest CT scan. *Respir Med.* 2021; 181: 106384. DOI: 10.1016/j.rmed.2021.106384
- [54] Tana C., Ricci F., Coppola M.G., et al. Prognostic Significance of Chest Imaging by LUS and CT in COVID-19 Inpatients: The ECOVID Multicenter Study. *Respiration.* 2022; 101(2): 122–31. DOI: 10.1159/000518516
- [55] Konopka K.E., Nguyen T., Jentzen J.M., et al. Diffuse alveolar damage (DAD) resulting from coronavirus disease 2019 Infection is Morphologically Indistinguishable from Other Causes of DAD. *Histopathology.* 2020; 77(4): 570–8. DOI: 10.1111/his.14180
- [56] Vasquez-Bonilla W.O., Orozco R., Argueta V., et al. A review of the main histopathological findings in coronavirus disease 2019. *Hum Pathol.* 2020; 105: 74–83. DOI: 10.1016/j.humpath.2020.07.023
- [57] Ito G.N.W., Rodrigues V.A.C., Hümmelgen J., et al. COVID-19 pathophysiology and ultrasound imaging: A multiorgan review. *J Clin Ultrasound.* 2022; 50(3): 326–38. DOI: 10.1002/jcu.23160
- [58] Tomaszefski J.F. Pulmonary pathology of acute respiratory distress syndrome. *Clin Chest Med.* 2000; 21(3): 435–66. DOI: 10.1016/s0272-5231(05)70158-1
- [59] Samsonova M.V., Chernyaev A.L., Omarova Z.R., et al. Features of pathological anatomy of lungs at COVID-19. *Pulmonologiya.* 2020; 30(5): 519–32. DOI: 10.18093/0869-0189-2020-30-5-519-532
- [60] Laforge M., Elbim C., Frère C., et al. Tissue damage from neutrophil-induced oxidative stress in COVID-19. *Nat Rev Immunol.* 2020; 20(9): 579. DOI: 10.1038/S41577-020-00425-7
- [61] Almeida Monteiro R.A., de Oliveira E.P., Nascimento Saldiva P.H., et al. Histological-ultrasonographical correlation of pulmonary involvement in severe COVID-19. *Int Care Med.* 2020; 46(9): 1766–8. DOI: 10.1007/S00134-020-06125-z